

RESEARCH ARTICLE | JUNE 20 2023

Comparison of BCl_3 , TiCl_4 , and SOCl_2 chlorinating agents for atomic layer etching of TiO_2 and ZrO_2 using tungsten hexafluoride

Special Collection: [Celebrating the Achievements and Life of Joe Greene](#)

Holger Saare; Wenyi Xie  ; Gregory N. Parsons  



J. Vac. Sci. Technol. A 41, 042602 (2023)

<https://doi.org/10.1116/6.0002708>



View
Online



Export
Citation

Articles You May Be Interested In

Ultrathin ZrO_2 thickness control on $\text{TiO}_2/\text{ZrO}_2$ core/shell nanoparticles using ZrO_2 atomic layer deposition and etching

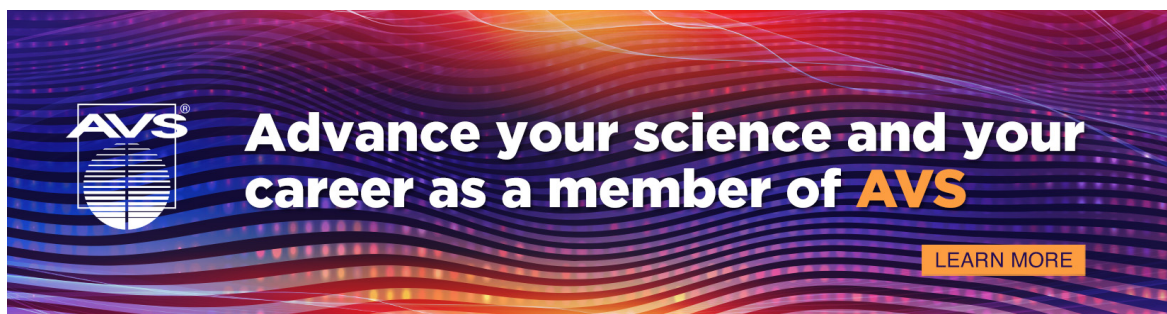
J. Vac. Sci. Technol. A (August 2024)

Raman Spectroscopy of Carbon Nanotube-Polyaniline and Functionalized CNT/ SOCl_2 Films

AIP Conf. Proc. (October 2003)

Effect of crystallinity on thermal atomic layer etching of hafnium oxide, zirconium oxide, and hafnium zirconium oxide

J. Vac. Sci. Technol. A (February 2020)



Comparison of BCl_3 , TiCl_4 , and SOCl_2 chlorinating agents for atomic layer etching of TiO_2 and ZrO_2 using tungsten hexafluoride

Cite as: J. Vac. Sci. Technol. A 41, 042602 (2023); doi: 10.1116/6.0002708

Submitted: 22 March 2023 · Accepted: 12 May 2023 ·

Published Online: 20 June 2023



View Online



Export Citation



CrossMark

Holger Saare,¹ Wenyi Xie,²  and Gregory N. Parsons^{1,2,a} 

AFFILIATIONS

¹ Department of Physics, North Carolina State University, Raleigh, North Carolina 27695

² Department of Chemical and Biomolecular Engineering, North Carolina State University, Raleigh, North Carolina 27695

Note: This paper is part of the Special Topic Collection Celebrating the Achievements and Life of Joe Greene.

a) Author to whom correspondence should be addressed: gnp@ncsu.edu

ABSTRACT

Recent advances in the semiconductor industry have created an exigency for processes that allow to deposit and etch material in conformal matter in three-dimensional devices. While conformal deposition is achieved using atomic layer deposition (ALD), conformal etching can be accomplished by thermal atomic layer etching (ALE) which, like ALD, proceeds via a binary sequence of self-limiting reactions. This study explores ALE of TiO_2 and ZrO_2 using WF_6 as a fluorinating agent, and BCl_3 , TiCl_4 , or SOCl_2 as a co-reactant. The effect of co-reactant chemistry was studied using atomic force microscopy, *in situ* ellipsometry, and *in vacuo* Auger electron spectroscopy measurements along with thermodynamic modeling. All three co-reactants exhibited saturation and etch rates increasing with temperature. At 170 °C, TiO_2 can be etched using WF_6 with BCl_3 , TiCl_4 , or SOCl_2 , and the etching proceeds at 0.24, 0.18, and 0.20 nm/cycle, respectively. At 325 °C, ZrO_2 ALE can occur using these same reactants, proceeding at 0.96, 0.74, and 0.13 nm/cycle, respectively. A higher temperature is needed for ZrO_2 ALE versus TiO_2 because the ZrCl_4 product is less volatile than the corresponding TiCl_4 . During ZrO_2 and TiO_2 etching using BCl_3 or TiCl_4 , boron oxide or titanium oxide intermediate layers, respectively, were formed on the surface, and they were subsequently removed by WF_6 . In contrast, for ALE of TiO_2 using SOCl_2 , a similar intermediate layer is not observed. This study broadens the understanding of co-etchants role during thermal ALE and expands the range of reactants that can be used for vapor etching of metal oxides.

Published under an exclusive license by the AVS. <https://doi.org/10.1116/6.0002708>

I. INTRODUCTION

An etching step is an essential procedure in semiconductor manufacturing to remove unwanted materials from the sample substrate. This is done, for example, to etch trenches, shape via holes, or create patterns. While wet etching methods were historically used for microfabrication, continuous device miniaturization has limited their use due to their isotropic nature and hard to control etch rates.¹ As such, dry etching technologies are mainly used in advanced processes due to their more precise feature size control and capability to achieve higher aspect ratios.^{1,2} Dry etching technologies include processes that employ physical etching (such as reactive ion etching, sputter etching, or ion milling) or chemical etching [chemical vapor etching (CVE), atomic layer etching].

Vapor etching is conventionally used in the semiconductor industry to etch the sacrificial layer present in a device. For example, xenon difluoride (XeF_2) or HF vapor combined with water as a catalyst is employed to remove a silicon oxide layer in silicon MEMS devices.^{3–8} In addition to SiO_2 , CVE of other materials, such as TiO_2 , Al_2O_3 , and Cu, have been reported using WF_6 , HF/Sn(acac)₂, and O_2/hfach , respectively.^{9–11} However, chemical vapor etching of many materials is limited due to the formation of metal fluorides or other species that are nonvolatile at the reaction temperature. This has enabled the development of atomic layer etching, ALE, which is a self-limiting two-step process.^{12–14} The ALE sequence involves a surface modification step followed by a removal step, where either step can be driven by thermal reactions or by plasma treatment and/or ion bombardment. While the mechanisms for plasma and

18 July 2023 11:46:54

ion-based methods have been studied extensively, thermally driven ALE is gaining traction because it can enable isotropic and conformal etching with molecular scale precision, required for complex nanopatterns.^{15,16}

Thermal ALE processes have been successfully developed for materials including Al₂O₃,^{17–20} Si,^{21,22} SiO₂,^{23,24} HfO₂,^{25–27} ZnO,^{28,29} Cu,^{30–32} W,^{33,34} TiN,^{10,35,36} and others.^{37–46} Mechanisms developed for thermal ALE include fluorination/ligand-exchange, conversion/etch, oxidation/fluorination, and others.¹⁶ ZrO₂ has been etched using HF as a fluorinating agent, with Sn(acac)₂, AlCl(CH₃)₂ or SiCl₄ as co-reactants to volatilize the fluorinated surface layer through ligand exchange.¹⁰ Similarly, TiO₂ ALE has been developed using alternating doses of WF₆ and BCl₃.⁹ In this process, the WF₆ fluorinates the surface, creating WO_xF_y/TiO_vF_z layer that is volatile at temperatures above 200 °C, enabling CVE of TiO₂. At T < 200 °C introducing a BCl₃ exposure step allows TiO₂ etching to proceed via ALE. At low temperature, BCl₃ reacts with the nonvolatile WO_xF_y/TiO_vF_z via ligand exchange, producing volatile TiCl₄ and WOCl₄ products and a thin solid B₂O₃ layer, which is subsequently etched during the following WF₆ exposure step.

In situ analysis techniques allow the monitoring of the etching process under the practical conditions without exposing the sample to atmosphere or interrupting the experiment. *In situ* ellipsometry can be employed to actively monitor the etch rate or changes in the optical properties of the material being etched. It has been previously utilized to analyze ALE of various materials, including GaN,⁴⁶ Ga₂O₃,⁴¹ ZnO,²⁹ Cu,³⁰ and W.³⁴ To confirm the conversion or removal of an element, *in situ* chemical analysis methods, such as x-ray photoelectron spectroscopy (XPS) or Auger electron spectroscopy (AES), can be used. For example, *in situ* XPS has been used to study the efficiency of acacH versus hfacH for ALE when combined with chlorine gas and to study the mechanism of Fe ALE, when etched using Cl₂ and acacH.³⁷ Similarly, *in situ* AES has been utilized to study the ALE of GaAs when etched using Cl₂ exposure followed by flash heating⁴⁷ and to investigate both thermal and plasma enhanced ALE of Al₂O₃ and HfO₂ films.⁴⁸

In this article, the etching characteristics of thionyl chloride (SOCl₂), titanium tetrachloride (TiCl₄), and boron trichloride (BCl₃) are compared when coupled with WF₆ in a fluorination/ligand-exchange atomic layer etching process. The processes are characterized using *in situ* ellipsometry, *in vacuo* AES, and atomic force microscopy (AFM). The results indicate that while all three chlorinating precursors lead to ALE of ZrO₂ and TiO₂, the reaction byproducts differ, leading to distinct etch rates and temperature windows. Previously, SOCl₂ has been shown to etch TiN.⁴⁹ Although WF₆/BCl₃ are known to enable ALE of TiO₂, the drawback of using BCl₃ is that the reaction results in a solid B₂O₃ layer, which can be removed by subsequent WF₆ exposure.⁹ In contrast, we show that exposing TiO₂ to SOCl₂ results only in volatile species, leaving a clean oxide surface after the SOCl₂ step. In addition, we show that at higher temperatures (>190 °C) the exposure of SOCl₂ leads to vapor etching of TiO₂ by converting the metal oxide to volatile TiCl₄ and SO₂ species, while ZrO₂ is not etched due to the low volatility of ZrCl₄. These results improve our understanding of the importance of co-reactant selection during atomic layer etching processes and expand the range of reactants and materials that can be used for vapor etching of metal oxides.

II. EXPERIMENTAL DETAILS

A. Deposition/etch reactor

The etching processes were carried out in a lab-built warm-walled chamber system as shown in Fig. 1. The system consists of a processing chamber, equipped with an *in situ* multi-wavelength ellipsometer, a load lock and an ultrahigh vacuum analysis chamber, equipped with AES. The samples are introduced into the system on a 2-in. stainless steel puck, which can be transferred between the chambers using linear transfer arms. During processing, the sample was heated to a constant temperature using two PID (Proportional-Integral-Derivative) controlled halogen lamps. Argon (99.999% purity, Arc3 gases) was used as a carrier and purge gas at a flow rate of 95 SCCM, as set by mass-flow controllers. The processing chamber was pumped out using a turbo pump (Seiko-Seiki STP-300C) and a backing pump (Alcatel 2021a) with a throttle valve located before the turbo pump used to control the operating pressure, which was set at 400 mTorr.

B. Substrate preparation and etching

The TiO₂ substrates used in this study were deposited in the same chamber immediately before the etching process using TiCl₄ (99% purity, Strem Chemicals) and DI-H₂O. Titania was deposited on chemical Si oxide at 170 °C. The zirconia thin films were deposited on alumina thin films using the Ultratech Fiji G2 system. The deposition was carried out at 250 °C using tetrakisdimethylammonia-zirconium (TDMA-Zr) and DI-H₂O as precursors. All substrates were purged in argon and held at processing temperature for 30 min to allow the conditions to stabilize before etching. Tungsten hexafluoride (99.99% purity, Galaxy Chemical), boron trichloride (99.9% purity, Matheson), thionyl chloride (99% purity, MilliporeSigma), and titanium tetrachloride (99% purity, Strem Chemicals) were used as etchants. The ALE cycles followed a dosing sequence of WF₆/purge/pump/pressurize/x/purge/pump/pressurize with timings of 0.08/15/10/15/x/15/10/15 s, where x stands for BCl₃, TiCl₄, or SOCl₂ with dosing times of 0.08, 0.1, or 0.2 s, respectively. During the pump step, the throttle valve to a turbo pump is opened completely to evacuate the chamber to a base pressure of 10⁻⁵ Torr. The subsequent pressurization step is

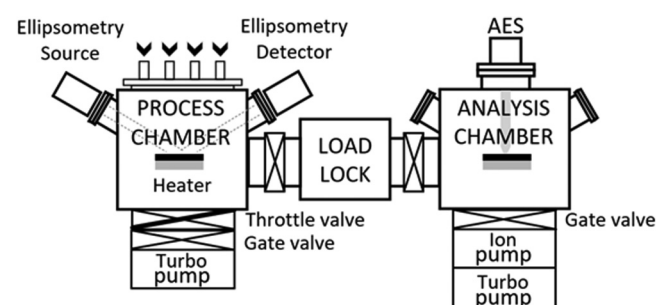


FIG. 1. Schematic view of the warm-walled chamber system. The system consists of a processing chamber, equipped with an *in situ* ellipsometer and of an analysis chamber with an *in situ* Auger electron spectrometer.

necessary to bring the system back to the stable operating pressure of 400 mTorr. The vapor etching processes followed the same sequence, but without the WF₆ dosing step.

C. Process characterization

The changes in film optical thicknesses during etching processes were monitored using *in situ* multiwavelength ellipsometer (Film Sense FS-1). The ellipsometer was set at 70° ± 1° incident angle and a data point was obtained after every etching cycle. For greater accuracy, the measurement lasted 10 s and the reported data is an average of the signal collected during that period. The optical film thickness was calculated by fitting the obtained raw ψ and Δ values to a Cauchy model.

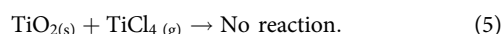
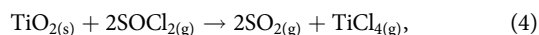
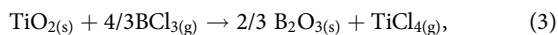
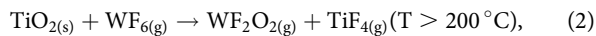
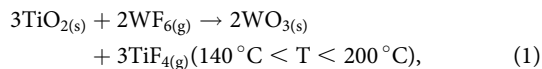
In vacuo AES measurements were performed to monitor the elemental composition changes of the metal oxides during etching. The AES system employs a coaxial cylindrical mirror analyzer (Perkin Elmer PHI 10-155) and a 3 kV electron beam. The ultra-high vacuum analysis chamber was kept at a pressure of ~10⁻¹⁰ Torr using an ion pump (Digitel 500 220 l/s) and a turbo pump (Edwards EXT501).

The morphology of samples was examined using AFM. The surface roughness data were acquired using Asylum MFP-3D Classic AFM in tapping mode. A silicon probe with a cantilever length of 125 μm and a force constant of 40 N m⁻¹ was used at ambient conditions.

III. ETCH SPECIES REACTIONS ON TiO₂ AND ZrO₂

A. Thermodynamic modeling of reactant exposure on TiO₂ and ZrO₂

Thermodynamic analysis⁵⁰ was used to predict reactions between gas phase reactants (WF₆, BCl₃, SOCl₂, and TiCl₄) and solid TiO₂ and ZrO₂ in the temperature range of 25–400 °C. The output gives the resulting equilibrium composition by minimizing the system's free energy. It is important to note that as it is a thermodynamic calculation, it does not include kinetic effects and presumes a closed system. The calculations were done at a pressure of 1.5 Torr with the initial molecular ratios of TiO₂ to WF₆, BCl₃, SOCl₂, and TiCl₄ set at 1:1, 0.75:1, 1:1, and 0.5:1, respectively. Figures 2(a)–2(d) show that when TiO₂ reacts with WF₆, BCl₃, SOCl₂, and TiCl₄, respectively, the expected primary reactions are

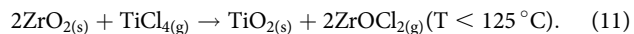
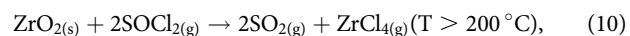
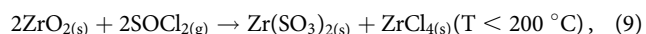
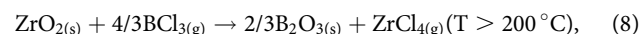
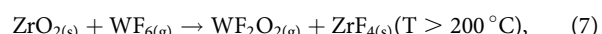
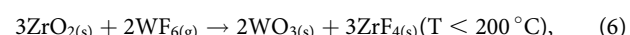


At temperatures between ~140 and 200 °C, exposing TiO₂ to

WF₆ forms TiF₄ vapor and solid WO₃ [reaction (1)] whereas at higher temperatures [reaction (2)] the expected products are gaseous TiF₄ and WO₂F₂, consistent with chemical vapor etching. Both BCl₃ and SOCl₂ [reactions (3) and (4)] are expected to form volatile TiCl₄, and the BCl₃ leaves solid B₂O₃ [reaction (3)] whereas SOCl₂ forms SO₂ vapor [reaction (4)].

B. Thermodynamic modeling of reactant exposure on ZrO₂

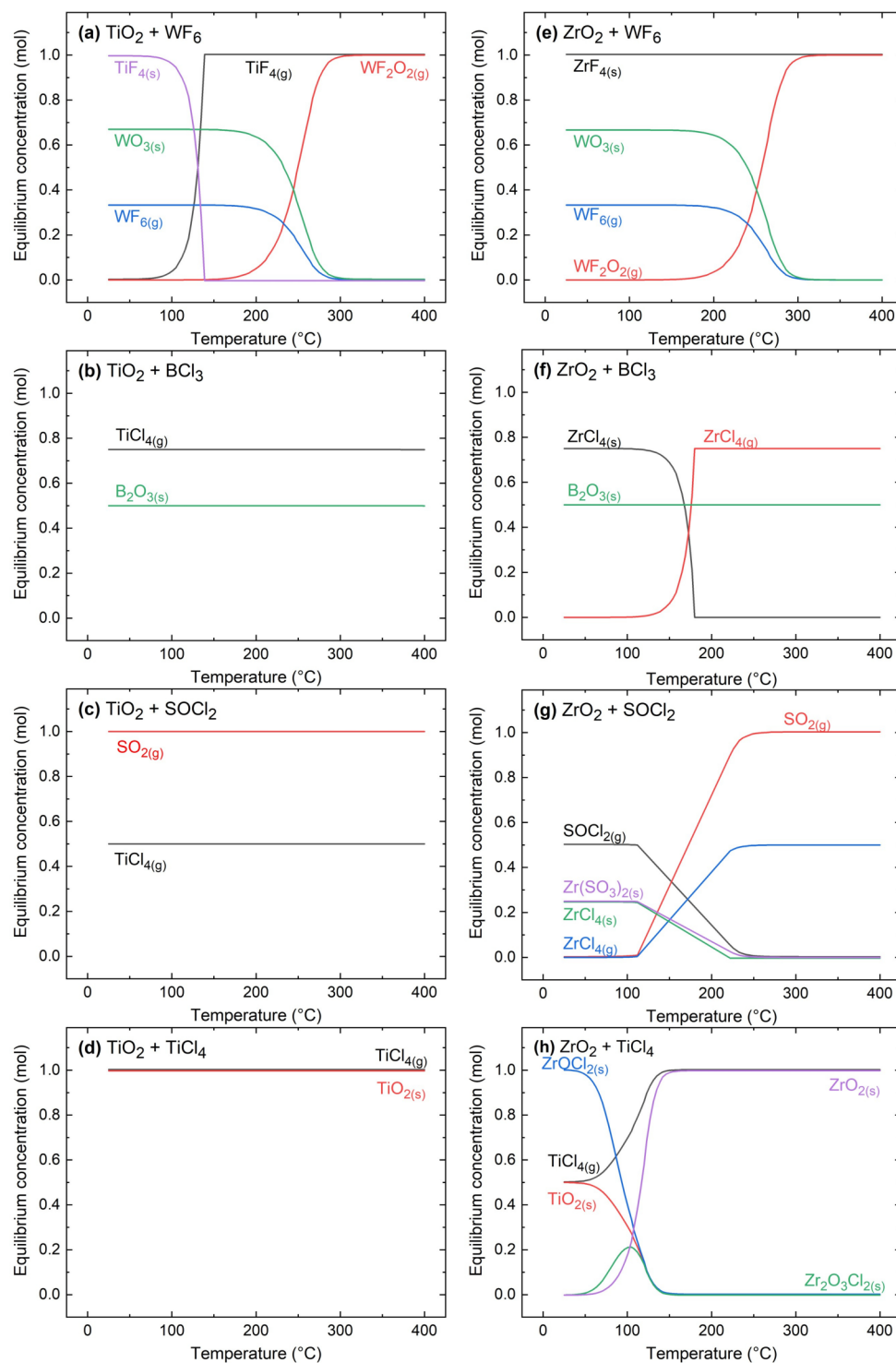
Figures 2(e)–2(h) show analogous predicted results for ZrO₂ reacting with WF₆, BCl₃, SOCl₂, and TiCl₄. The calculations were done with initial molecular ratios of ZrO₂ to WF₆, BCl₃, SOCl₂, and TiCl₄ set at 1:1, 0.75:1, 1:1, and 0.5:1, respectively. The predicted primary reactions are



When WF₆ reacts with ZrO₂ at T < 200 °C [reaction (6)], the reaction proceeds similarly as on TiO₂, producing solid ZrF₄ and solid WO₃. Also analogous to the reaction on TiO₂, at T > 200 °C, ZrO₂ reacting with WF₆ is expected to yield gaseous WO₂F₂ [reaction (7)]. However, unlike the reaction on TiO₂, the resulting ZrF₄ is expected to remain solid at all temperatures studied. At temperatures above about 200 °C, exposing ZrO₂ to BCl₃ or SOCl₂ [reactions (8) and (10)] produces volatile ZrCl₄. For SOCl₂ at T > 200 °C, the chlorination of ZrO₂ also yields volatile SO₂ [reaction (10)]. Therefore, exposing ZrO₂ to SOCl₂ at T > 200 °C is expected to lead to spontaneous chemical vapor etching. In contrast, exposing ZrO₂ to BCl₃ [reaction (8)] forms solid B₂O₃, and this solid layer is expected to inhibit continuous etching of ZrO₂. However, at T > 200 °C, as shown below, the B₂O₃ can be removed in a subsequent WF₆ exposure step to achieve ZrO₂ atomic layer etching. At lower temperatures, <200 °C, exposing ZrO₂ to SOCl₂ [reaction (9)] forms a solid Zr(SO₃)₂/ZrCl₄ intermediate layer. On the other hand, at T < 125 °C, reacting ZrO₂ with TiCl₄ [reaction (11)] is expected to convert ZrO₂ into solid TiO₂ and produce vapor ZrOCl₂. Interestingly, at T > 125 °C, like in the case of TiCl₄ + TiO₂, the thermodynamic analysis indicates that TiCl₄ is not expected to react with ZrO₂.

C. *In situ* ellipsometry study of reactions on TiO₂

The effect of exposure of individual reactants (WF₆, BCl₃, SOCl₂, TiCl₄) on the thickness of the titania and zirconia thin films was analyzed experimentally over a range of reaction temperatures



18 July 2025 11:46:54

FIG. 2. Expected equilibrium species determined by thermodynamic modeling in the temperature range from 25 to 400 °C for [(a) and (e)] 1 mol $\text{TiO}_2/\text{ZrO}_2$ and 1 mol WF_6 , [(b) and (f)] 0.75 mol $\text{TiO}_2/\text{ZrO}_2$ and 1 mol BCl_3 , [(c) and (g)] 0.5 mol $\text{TiO}_2/\text{ZrO}_2$ and 1 mol SOCl_2 , and [(d) and (h)] 1 mol $\text{TiO}_2/\text{ZrO}_2$ and 1 mol TiCl_4 .

using *in situ* ellipsometry. Before etching, the TiO₂ film was deposited on a silicon coupon by ALD at 170 °C using TiCl₄ and H₂O. The deposition was done in the same reactor used for etching, and the films were maintained in the reactor environment between the deposition and etching steps. The resulting change in thickness of the TiO₂ for each reactant is plotted in Figs. 3(a)–3(d) as a function of the number of reactant dose steps. The data show that TiO₂ is etched by WF₆ exposure at temperatures ≥200 °C, consistent with the previous results.⁹ At temperatures less than 200 °C, the thickness shows a small decrease during initial doses, with no change during subsequent exposures. The data for WF₆ exposure on TiO₂ are consistent with the thermodynamic analysis described above where spontaneous chemical vapor etching is expected at T > 200 °C [reaction (2)] but not expected at T < 200 °C due to the formation of solid WO₃ [reaction (1)].

For BCl₃ and TiCl₄ exposures, TiO₂ shows no apparent thickness change after the first dose in the temperature range 160–240 °C. However, exposing TiO₂ to SOCl₂ at T > 220 °C leads to a thickness decrease. Like WF₆, the etch rate using SOCl₂ increases as the temperature increases. At T > 200 °C, the experimental results for SOCl₂ reaction on TiO₂ are consistent with the thermodynamic analysis showing production of volatile SO₂ and TiCl₄ [reaction (4)]. Thermodynamically, SOCl₂ is also expected to etch TiO₂ at T < 200 °C [reaction (4)] but the experiment shows limited etching, likely due to slow reaction kinetics at low temperatures.

D. *In situ* ellipsometry study of reactions on ZrO₂

For analysis of ZrO₂ etching, ZrO₂ films were deposited by ALD at 250 °C using TDMA-Zr and H₂O. To avoid possible reactions between the WF₆ and the underlying Si after ZrO₂ is fully etched, the silicon substrates were pretreated with 50 cycles of ALD Al₂O₃ before the ZrO₂ ALD.⁵¹ For the ZrO₂ etching experiments, the deposition was carried out in a separate reactor and the starting ZrO₂ sample was transferred in air to the etch reactor. The results of all individual exposures on ZrO₂ are plotted in Figs. 3(e)–3(h). Exposing zirconia to WF₆ leads to a thickness decrease, but unlike the reaction on TiO₂, the thickness decrease stopped after a few initial cycles. The initial decrease of ZrO₂ thickness upon WF₆ exposure is consistent with the thermodynamic analysis [reaction (7)] showing formation of volatile WO₂F₂ species and a solid ZrF₄. The solid ZrF₄ likely inhibits further reactions with WF₆.

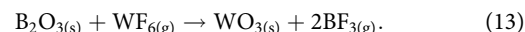
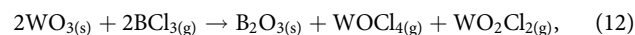
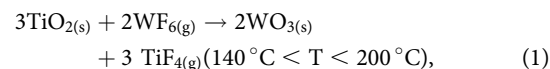
For all temperatures studied, exposing ZrO₂ to BCl₃, SOCl₂, or TiCl₄ leads to no significant change in the film thickness [Figs. 3(f)–3(h)]. The results for BCl₃ and TiCl₄ are consistent with the thermodynamic analysis [reactions (8) and (11)]. However, at T > 200 °C, ZrO₂ is expected to be etched by SOCl₂ [reaction (10)]. The lack of reaction suggests a key step in the reaction mechanism is kinetically limited.

IV. ATOMIC LAYER ETCHING REACTIONS ON TiO₂ AND ZrO₂

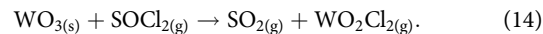
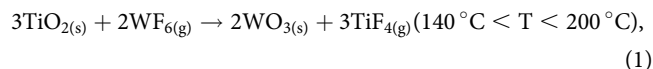
A. Thermodynamic modeling of TiO₂ ALE process sequence

The results shown above demonstrate that at elevated temperatures, WF₆ and SOCl₂ will react with TiO₂ to produce volatile etch products via chemical vapor etching. At lower temperatures, the

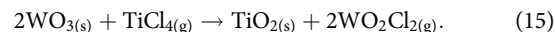
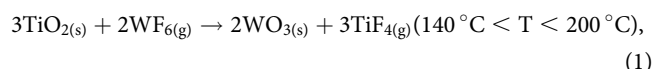
formation of solid surface species can be exploited for a more controlled two-step atomic layer etch process. For example, analysis in Fig. 2(a) shows that at T < 200 °C, exposing TiO₂ to WF₆ is expected to form solid WO₃. Starting from this modified surface, we applied the thermodynamic analysis to explore further reactions that could proceed with the BCl₃, SOCl₂, and TiCl₄ chlorinating reagents, and the results are plotted in Figs. 4(a)–4(c). When BCl₃ reacts with solid WO₃ [reaction (12)] the expected products are volatile WOCl₄ and WO₂Cl₂ along with solid B₂O₃. B₂O₃ can be removed during the subsequent WF₆ exposure [reaction (13)] as shown in Fig. S1 in supplementary material,⁵² enabling well-controlled ALE, where the full ALE cycle includes reaction (1) repeated from above,



For some applications, the resulting B₂O₃ intermediate layer may be undesirable. The analysis suggests that exposing WO₃ to SOCl₂ [reaction (14)] will form volatile SO₂ and WO₂Cl₂ species leaving a clean TiO₂ surface. The ALE cycle then follows:

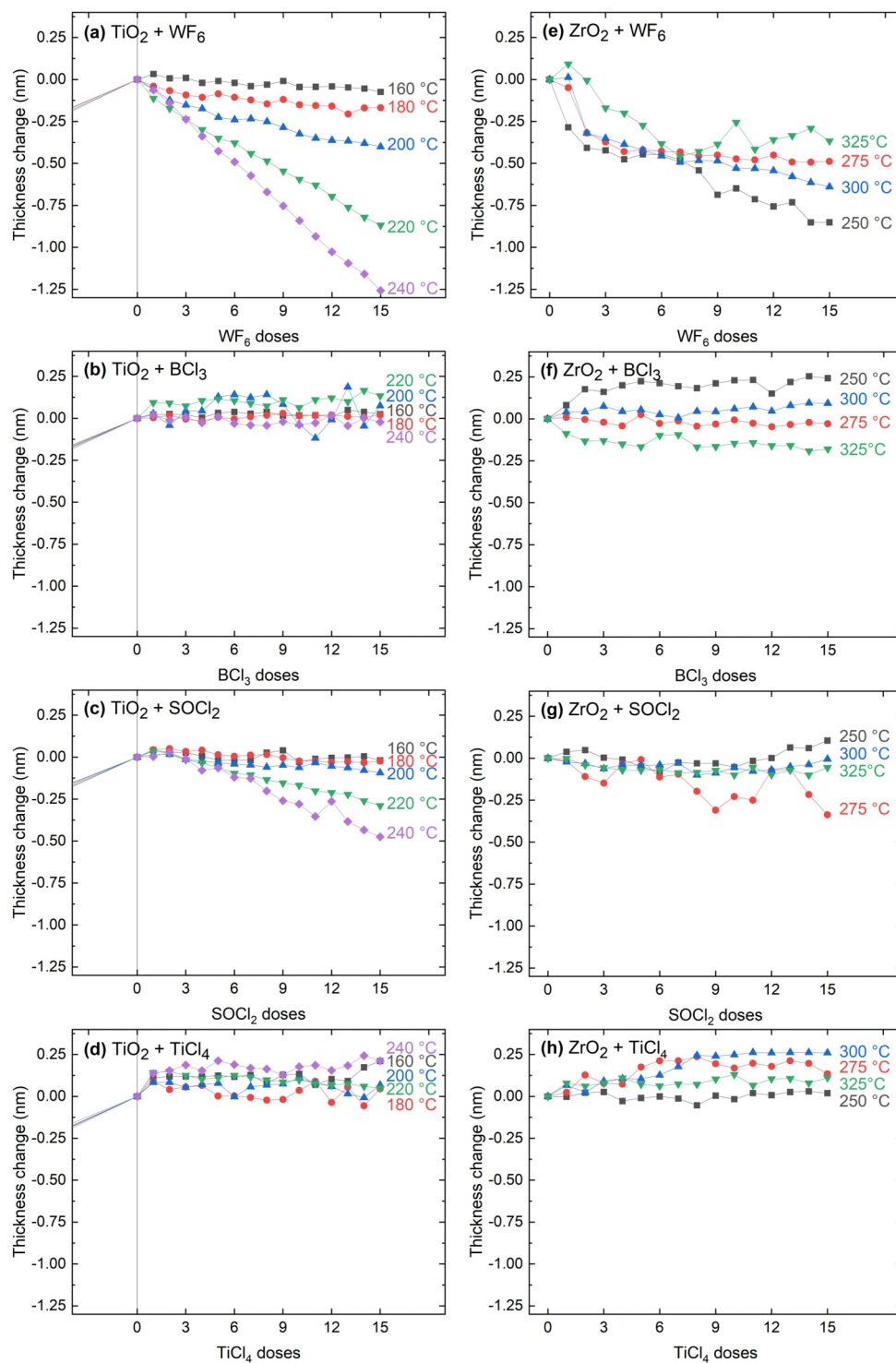


A similar sequence using WF₆ and TiCl₄ gives a very different result. Reacting WO₃ with TiCl₄ is expected to convert WO₃ to back to solid TiO₂ and vapor WO₂Cl₂ [reaction (15)]. This reaction sequence does not produce ALE, but instead, the original TiO₂ which was converted to WO₃ is effectively “re-converted” back to “new” TiO₂ from TiCl₄,



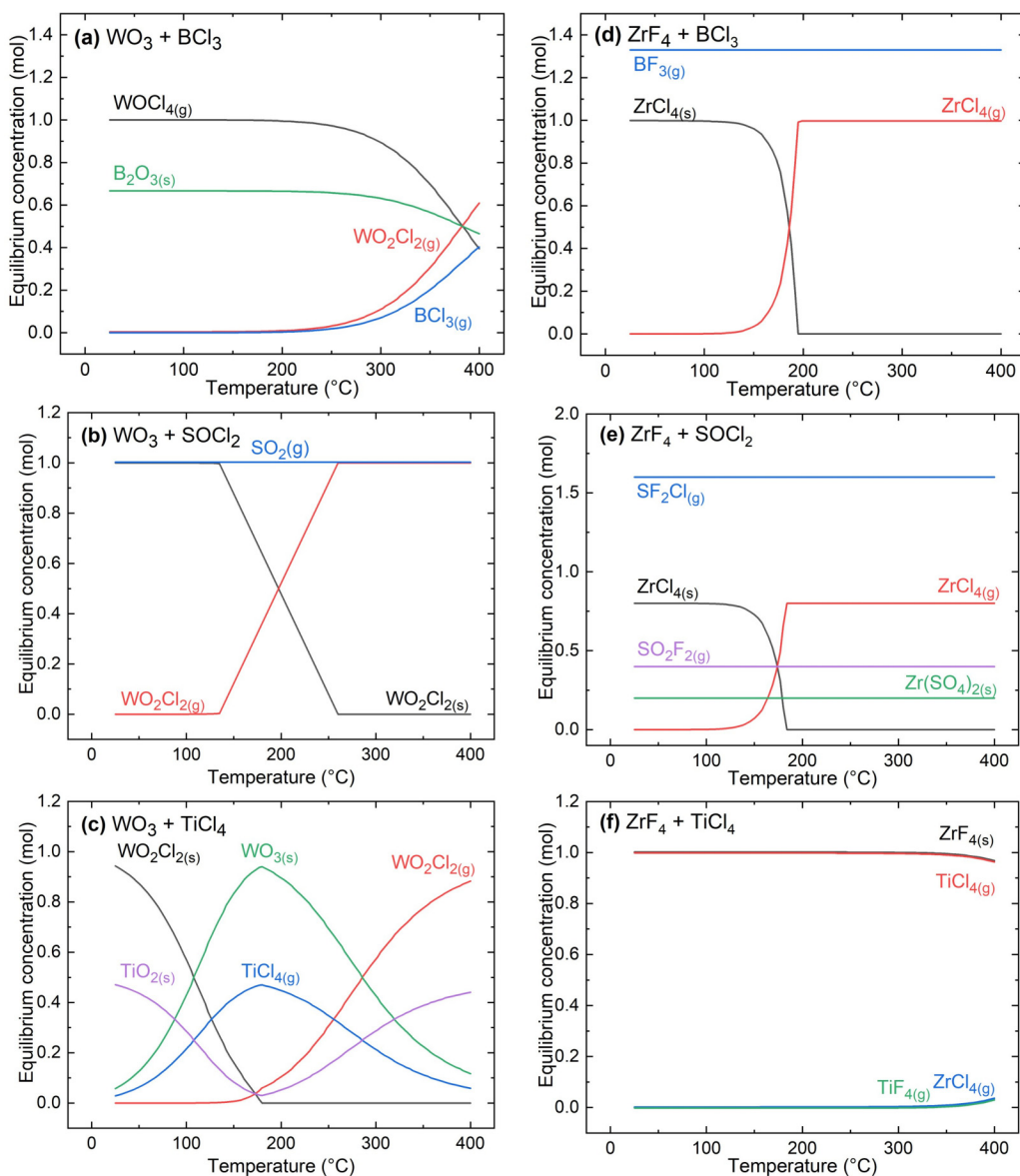
B. Thermodynamic modeling of ZrO₂ ALE process sequence

As shown above, at T > 200 °C, exposing ZrO₂ to WF₆ [reaction (7)] is expected to form solid ZrF₄. To create an ALE sequence, we used thermodynamic analysis to test possible reactions between ZrF₄ and the chlorinating reagents, and the results are plotted in Figs. 4(d)–4(f). Reacting ZrF₄ with BCl₃ is predicted to result in gaseous BF₃ and ZrCl₄ products at temperatures above 200 °C [reaction (16)]. Therefore, a possible ALE sequence for ZrO₂ uses WF₆ and BCl₃ at T > 200 °C, where reaction (7) is



18 July 2025 11:46:54

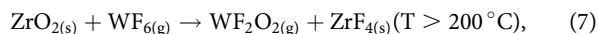
FIG. 3. Thickness change of TiO_2 and ZrO_2 thin films when exposed to WF_6 [(a) and (e)], BCl_3 [(b) and (f)], SOCl_2 [(c) and (g)], or TiCl_4 [(d) and (h)] doses at various temperatures as measured by *in situ* ellipsometry.



18 July 2023 11:49:54

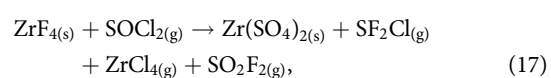
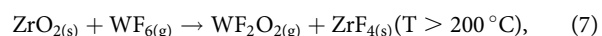
FIG. 4. Expected equilibrium species determined by thermodynamic modeling in the temperature range from 25 to 400 °C for 1 mol WO_3 reacting with (a) 4/3 mol BCl_3 , (b) 1 mol TiCl_4 , (c) 1 mol SOCl_2 , and for 1 mol ZrF_4 reacting with (d) 4/3 mol BCl_3 , (e) 1 mol TiCl_4 , and (f) 2.4 mol SOCl_2 .

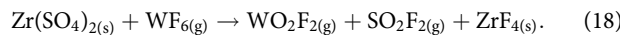
repeated from above:



For the case of ZrF_4 reacting with SOCl_2 [reaction (17)], the expected products include solid $\text{Zr}(\text{SO}_4)_2$ as well as SF_2Cl , ZrCl_4 , and SO_2F_2 vapor species. As shown in Fig. S1 in supplementary material,⁵² the solid $\text{Zr}(\text{SO}_4)_2$ layer can be removed by subsequent

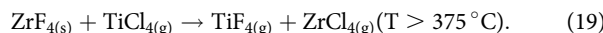
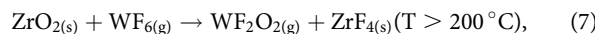
WF_6 exposure [reaction (18)], thereby allowing ALE, where again, the full ALE cycle includes reaction (7),





Note that reactions (17) and (18) are written in unbalanced form, suggesting that the solid layers formed on the surface, indicated as $\text{Zr}(\text{SO}_4)_{2(s)}$ and $\text{ZrF}_{4(s)}$, are likely more complex mixtures.

We next consider the possibility for ALE of ZrO_2 using WF_6 and TiCl_4 where the first step follows reaction (7) forming a solid ZrF_4 surface layer. For $T < \sim 375^\circ\text{C}$, TiCl_4 is not reactive with ZrF_4 , but for $T > 375^\circ\text{C}$ [reaction (19)] TiCl_4 undergoes ligand exchange to form volatile ZrCl_4 and TiF_4 . Therefore, ALE can be achieved using TiCl_4 as follows:

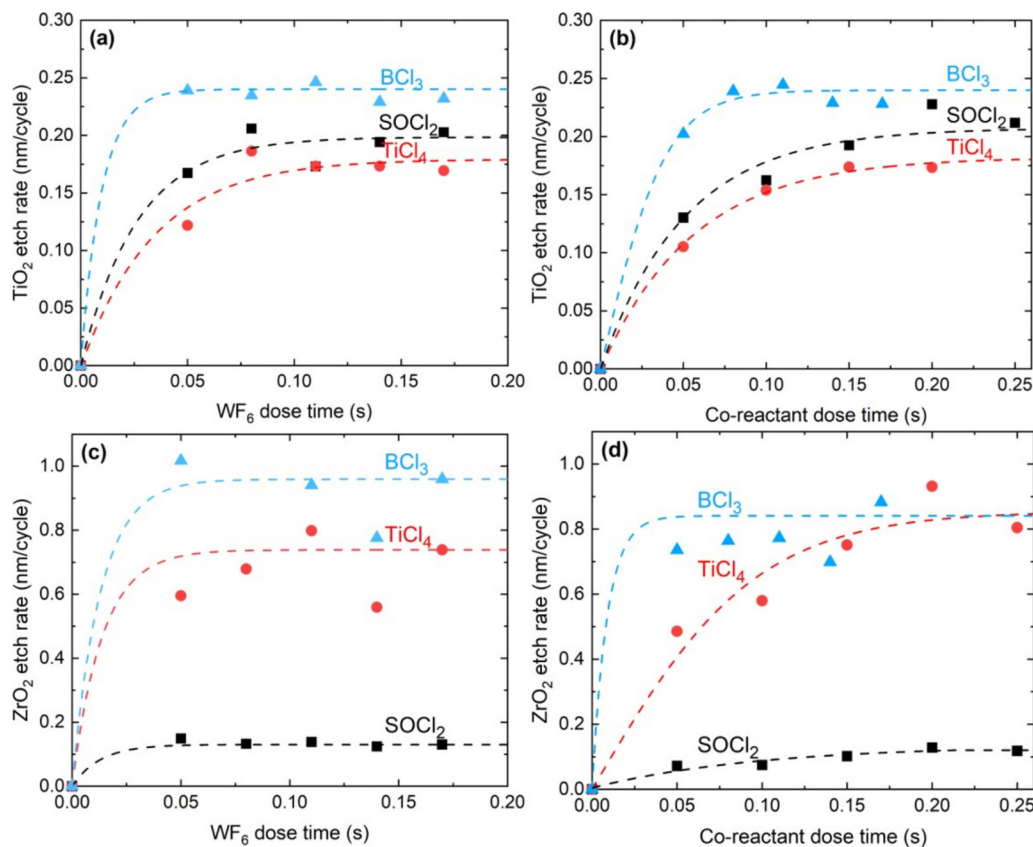


C. Chemical distinction between TiO_2 and ZrO_2 ALE

From the thermodynamic analysis above, TiO_2 ALE can proceed at low temperature with WF_6 and either BCl_3 or SOCl_2 (but not with TiCl_4), and at higher temperatures, ZrO_2 ALE can proceed with WF_6 and BCl_3 , SOCl_2 , or TiCl_4 . A key difference

between these processes is that TiO_2 ALE produces a solid oxide intermediate layer, WO_3 , [reaction (1)], whereas for ZrO_2 ALE, the solid intermediate layer is a halide, ZrF_4 [reaction (6) or (7)]. For both ALE sequences, this intermediate layer is subsequently removed by reaction with the chloride. For the TiO_2 and ZrO_2 ALE, the chloride reaction steps proceed very differently. For TiO_2 ALE using WF_6/BCl_3 , the solid WO_3 intermediate reacts with BCl_3 , for example, to produce solid B_2O_3 (i.e., a second intermediate) [reaction (12)], which is then removed by WF_6 [reaction (13)]. In contrast, for ZrO_2 ALE using WF_6/BCl_3 , the solid ZrF_4 intermediate reacts with BCl_3 to produce only gaseous ZrCl_4 and BF_3 [reaction (16)]. This surface will resemble clean ZrO_2 , with no second intermediate present.

This distinction is also expected when TiO_2 and ZrO_2 are exposed to $\text{WF}_6/\text{TiCl}_4$. On TiO_2 , when the WO_3 intermediate reacts with TiCl_4 [reaction (15)] the intermediate is “re-converted” back to solid TiO_2 . The overall reaction [i.e., reaction (1) + reaction (15)] shows a net loss of TiO_2 , consistent with ALE as shown in Fig. 5(a). Therefore, analogous with TiO_2 ALE with WF_6/BCl_3 , the re-converted solid TiO_2 layer is the “second intermediate,” which is removed by the following WF_6 dose. On ZrO_2 , also analogous with ZrO_2 ALE with WF_6/BCl_3 , reacting the ZrF_4 intermediate with TiCl_4



18 July 2025 11:46:54

FIG. 5. Saturation curves of etch rate dependence on WF_6 and co-reactant dose times for TiO_2 [(a) and (b)] and for ZrO_2 [(c) and (d)]. All TiO_2 etching processes were performed at 170°C and ZrO_2 etching at 325°C . The etch rate per cycle was determined by *in situ* ellipsometry over 10 ALE cycles.

at $T > 375^\circ\text{C}$ [reaction (19)] yields volatile TiF_4 and ZrCl_4 , with no second intermediate formed.

Interestingly, for etching using $\text{WF}_6/\text{SOCl}_2$, the distinction between TiO_2 and ZrO_2 reverses. On TiO_2 , the solid WO_3 intermediate reacts with SOCl_2 to form only volatile species [reaction (14)] leaving a clean TiO_2 surface, whereas during ZrO_2 etching, the intermediate solid ZrF_4 reacts with SOCl_2 [reaction (17)] to form both solid $\text{Zr}(\text{SO}_4)_{2(s)}$ (i.e., the second intermediate) and volatile $\text{ZrCl}_{4(g)}$. The solid $\text{Zr}(\text{SO}_4)_2$ is then converted back to $\text{ZrF}_{4(s)}$ by reacting with WF_6 [reaction (18)]. Therefore, similar to TiO_2 ALE by $\text{WF}_6/\text{TiCl}_4$, when $\text{WF}_6/\text{SOCl}_2$ is used for ZrO_2 ALE, the $\text{ZrF}_{4(s)}$ is partially removed as $\text{SO}_2\text{F}_{2(g)}$ and partially converted to $\text{Zr}(\text{SO}_4)_{2(s)}$ so that the net amount of Zr removed per ALE cycle is expected to be less than one stoichiometric ZrO_2 layer. This is consistent with the results in Figs. 5(c) and 5(d) showing a relatively small etch thickness per cycle for ZrO_2 ALE using $\text{WF}_6/\text{SOCl}_2$ compared to ALE using WF_6 with BCl_3 or TiCl_4 .

D. In situ ellipsometry analysis of TiO_2 and ZrO_2 ALE

In situ ellipsometry was used to obtain the saturation curves for etching of both TiO_2 and ZrO_2 . For this experiment, the dose time for each chlorinating agent was adjusted, keeping the dose time of the WF_6 dose fixed at 0.14 s, and the etch per cycle (EPC) was measured and plotted as a function of dose time. Similarly, for the WF_6 saturation, the dose times of $\text{BCl}_3/\text{TiCl}_4/\text{SOCl}_2$ were fixed at 0.14/0.25/0.25 s, while the dose time of WF_6 was varied in independent runs. The results are plotted in Fig. 5, where the EPC is presented as an average etch rate over 10 ALE cycles carried out at 170°C for TiO_2 and at 325°C for ZrO_2 . The ellipsometry data used to determine the EPC for each material are shown in Fig. S2 in supplementary material.⁵² It is evident that each of the chemistries showed reasonable reaction saturation, consistent with self-limiting atomic layer etching. The etch rates of TiO_2 saturated at 0.24, 0.18, and 0.20 nm/cycle for BCl_3 , TiCl_4 , and SOCl_2 , respectively. The saturated etch rates of ZrO_2 are 0.96, 0.74, and 0.13 nm/cycle, respectively. The EPC saturates at 0.08 s dosing times for WF_6 for all

processes, while 0.08 s is required for BCl_3 , and 0.2 s for both TiCl_4 and SOCl_2 to reach saturation on both TiO_2 and ZrO_2 .

Using *in situ* ellipsometry, the etched thickness per cycle was also measured over a range of reaction temperatures, where the dose times were fixed at the values obtained for saturation at 170 and 325°C for TiO_2 and ZrO_2 , respectively. Etch rates obtained at $T = 160\text{--}190^\circ\text{C}$ for TiO_2 and $250\text{--}325^\circ\text{C}$ for ZrO_2 are plotted in Fig. 6. The etch rate is strongly dependent on the temperature and increases linearly with temperature for all reactions studied. The etch rate of ZrO_2 using $\text{WF}_6/\text{SOCl}_2$ remains close to zero for temperatures $\leq 300^\circ\text{C}$, rising to ~ 0.16 nm/cycle at 325°C . We note that the thermodynamic analysis results in Fig. 4(e) and Fig. S1(b) in supplementary material⁵² indicate ZrO_2 etching by $\text{WF}_6/\text{SOCl}_2$ is expected to proceed at 300°C . The slow rate suggests some kinetic limitation, possibly corresponding to the fluorination of the surface $\text{Zr}(\text{SO}_4)_2$.

E. Elemental characterization of TiO_2 and ZrO_2 ALE

The atomic layer etching trends were further analyzed by *in situ* ellipsometry and *in vacuo* Auger electron spectroscopy. The resulting chemical compositions and optical thicknesses are plotted in Fig. 7 for titania and Fig. 8 for zirconia, while the raw AES spectra are shown in Fig. S3 in supplementary material.⁵² For these experiments, TiO_2 was first deposited using 40 ALD cycles on chemical silicon oxide at 170°C , resulting in an ~ 2 nm amorphous titania film. The etching was performed in the same reactor, also at 170°C , using WF_6 with BCl_3 , SOCl_2 , or TiCl_4 under saturated dose conditions (Fig. 5). As shown in Fig. 7, the TiO_2 thickness measured by ellipsometry decreases at a nearly constant EPC starting from the first ALE cycle, with some reduction in rate as the film thickness approaches zero. After 10 ALE cycles under the conditions used, ellipsometry measurements show <0.1 nm of TiO_2 remaining for all etchants studied.

The ellipsometry results were complemented by AES measurements. The AES was performed on different samples prepared under conditions identical to those for the ellipsometry study.

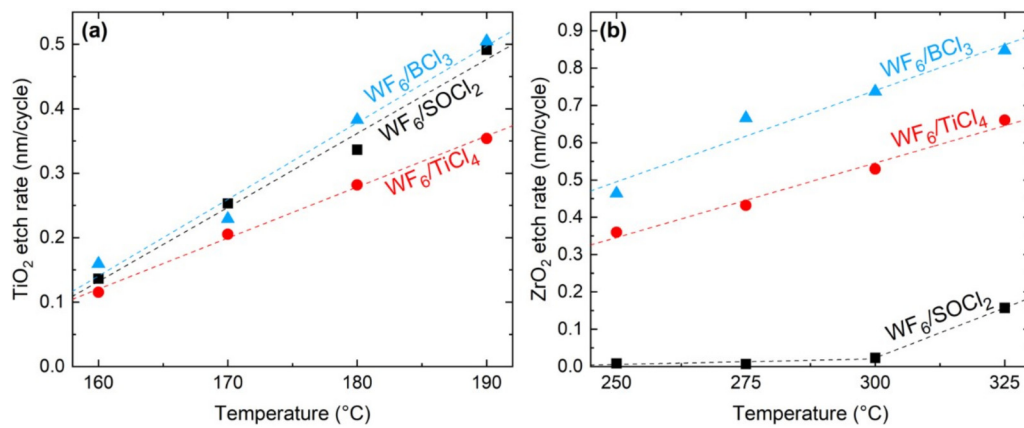


FIG. 6. Influence of substrate temperature on the etch rates during atomic layer etching of (a) TiO_2 and (b) ZrO_2 thin films.

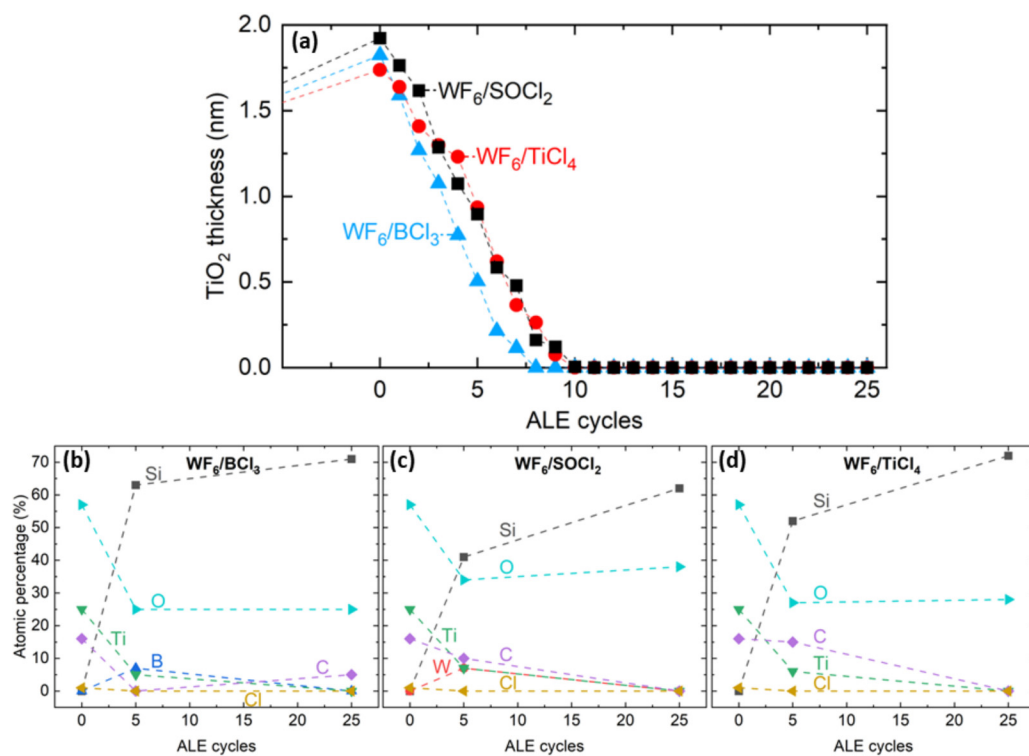


FIG. 7. (a) *In situ* ellipsometry and [(b)–(d)] Auger electron spectroscopy measurements of TiO_2 thermal ALE using WF_6 and BCl_3 , SOCl_2 , or TiCl_4 at 170°C . The ellipsometry data were collected after every ALE cycle, while AES measurements were done before etching and after 5 and 25 ALE cycles.

18 July 2023 11:46:54

For these runs, AES was performed on the as-deposited TiO_2 , and on newly prepared samples after 5 and 25 ALE cycles. In every case, the at. % of Ti decreases and the at. % of Si increases, with no Ti being detected after 25 ALE cycles, confirming that the ALE removes all of the TiO_2 film. After five WF_6/BCl_3 ALE cycles, 7 at. % of boron was detected, consistent with some boron oxide, as shown in Eq. (12). For the $\text{WF}_6/\text{SOCl}_2$ process, the surface showed 8 at. % of tungsten, consistent with the formation of tungsten oxide in Eq. (1). After 25 cycles, the AES shows no signals from these elements, indicating a clean etch surface.

Similar experiments were also performed for ZrO_2 etching. For these tests, approximately 3.5 nm thick zirconia films were deposited on silicon pretreated with ALD Al_2O_3 , and samples were loaded into the ALE reactor connected with the AES. The results of *in situ* ellipsometry and AES analysis are shown in Fig. 8. Using WF_6/BCl_3 or $\text{WF}_6/\text{TiCl}_4$, the ellipsometry shows that the etched thickness per cycle was constant starting from the first ALE cycle. Using $\text{WF}_6/\text{SOCl}_2$, the etch per cycle is also constant, with some enhanced etching observed during the first ALE cycle.

The AES results in Figs. 8(b)–8(d) confirm the etching of ZrO_2 at 325°C by all processes tried as evidenced by the decreasing concentration of Zr and appearance of Al from the underlying Al_2O_3 . Using BCl_3 as a co-etchant resulted in residue boron of 12 and 3 at. % after 5 and 25 ALE cycles, respectively. At this temperature, the thermodynamic analysis [Eq. (16)] indicates that boron

should be volatilized as $\text{BF}_{3(g)}$. The presence of residual boron, therefore, suggests that the rate of $\text{BF}_{3(g)}$ formation may be relatively slow. Another possibility is that BCl_3 reacts with small amounts of WO_3 in the film to form solid B_2O_3 [Eq. (12)]. This is also consistent with the minute W signal detected on the surface after ALE. After 25 cycles of WF_6/BCl_3 , ellipsometry indicates the ZrO_2 film is completely removed, while the AES shows a small signal corresponding to ~2 at. % of Zr remaining on the surface.

Using TiCl_4 with WF_6 for ALE of ZrO_2 at 325°C resulted in 1 at. % of Ti present after five ALE cycles. At 325°C , the formation of $\text{TiF}_{4(g)}$ may not be as fast as expected at higher temperatures [Eq. (19)]. After 25 cycles, no Ti was detected, but similar to that for BCl_3 , some Zr (3 at. %) remained present. Using SOCl_2 with WF_6 , due to its smaller etch per cycle, 15 at. % of Zr was detected on the surface after 25 ALE cycles. Moreover, 2 at. % of S was measured after both 5 and 25 cycles [Eq. (17)]. In the $\text{WF}_6/\text{SOCl}_2$ process, the change in ZrO_2 etch rate after the first ALE cycle can be attributed to a relatively slower reaction rate for WF_6 with solid $\text{Zr}(\text{SO}_4)_{2(s)}$ [reaction (18)] compared with the rate of reaction with the initial ZrO_2 surface [reaction (7)]. This is also confirmed by the S detected by AES after SOCl_2 exposure. While the ellipsometry indicated complete removal of the ZrO_2 film, in conflict with the Zr at. % measured by the AES, it is important to note that the underlying Al_2O_3 surface increases the complexity of the ellipsometric modeling and leads to a larger possible error.

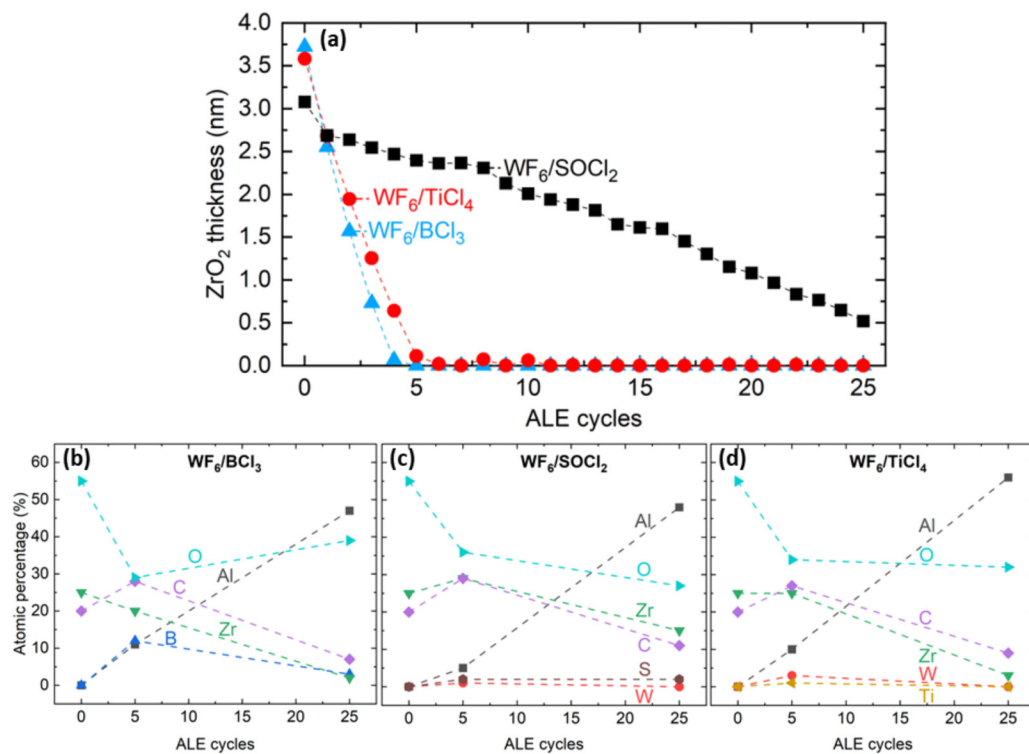


FIG. 8. (a) *In situ* ellipsometry and [(b)–(d)] Auger electron spectroscopy measurements of ZrO₂ thermal ALE using WF₆ and BCl₃, SOCl₂, or TiCl₄ at 325 °C. The ellipsometry data were collected after every ALE cycle, while AES measurements were done before etching and after 5 and 25 ALE cycles.

18 July 2023 114654

F. Surface morphology of metal oxides etched by ALE

The effect of atomic layer etching on the surface morphology of the samples was determined by atomic force microscopy. The calculated RMS surface roughness of the samples before etching and

after 5 and 25 ALE cycles is plotted in Fig. 9, while the surface images are shown in Fig. S4 in supplementary material.⁵² All the samples showed smooth surfaces with RMS surface roughness below 0.2 nm. Both titania and zirconia indicated surface smoothing by ALE processes. The measured roughness of TiO₂ decreased slightly with etching. Likewise, the RMS roughness of ZrO₂ dropped from ~200 to ~80 pm after 5 ALE cycles and remained constant after 25 cycles, indicating uniform etching and no residue in the shape of nuclei on the resulting surface for all processes studied.

V. CONCLUSIONS

This work describes the impact of co-reactant structure during thermal atomic layer etching of TiO₂ and ZrO₂ thin films. BCl₃, TiCl₄, and SOCl₂ were studied as co-etchants in a fluorination and ligand-exchange process when coupled with WF₆. In addition to ALE, it was shown that at temperatures above 200 °C, both WF₆ and SOCl₂ led to chemical vapor etching of TiO₂, while none of the reactants individually etched ZrO₂ due to the formation of a solid layer inhibiting further reaction.

The ALE behavior was shown to be strongly dependent on the co-etchant, temperature, and substrate material. Using *in situ* ellipsometry, the etch rate was shown to increase linearly with the temperature for all chemistries, except for ZrO₂ etching using WF₆/SOCl₂, which was limited by the unsuccessful removal of Zr

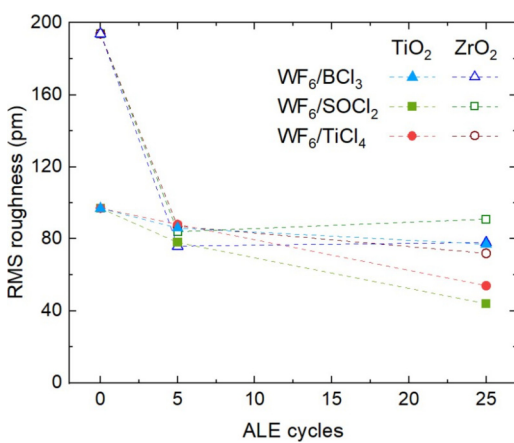


FIG. 9. RMS surface roughness evolution as a function of ALE cycles as measured by atomic force microscopy. The ALE of TiO₂ films was performed at 170 °C and the ZrO₂ films at 325 °C.

(SO₄)₂ by WF₆ exposure at temperatures ≤ 300 °C. The etch rates of TiO₂ at 170 °C were measured as 0.24, 0.18, and 0.20 nm/cycles for WF₆ and BCl₃, TiCl₄, or SOCl₂, respectively. The respective etch rates of ZrO₂ were 0.96, 0.74, and 0.13 nm/cycle at 325 °C. A higher temperature for ZrO₂ was needed due to a lower volatility of the formed ZrCl₄ compared to TiCl₄. All of the etchants studied showed saturating EPC as a function of etchant dosing times, characteristic of ALE processes.

The chemical reactions and the resulting compositions were analyzed by thermodynamic modeling and *in vacuo* AES. During TiO₂ ALE, the SOCl₂ exposure leads to volatile SO₂ and TiCl₄, in contrast to BCl₃ and TiCl₄, which result in solid B₂O₃ and TiO₂ on the surface, subsequently removed by WF₆ exposure. In contrast to TiO₂, all co-etchants led to the formation of solid species on ZrO₂ after exposure. BCl₃ resulted in B₂O₃, TiCl₄ in TiO₂, and SOCl₂ in Zr(SO₄)₂ at 325 °C. While the resulting layers are removed by subsequent WF₆ exposure, they could be undesirable reaction products when complete removal of the film is not desired. As such, co-reactant selection strongly affects the purity of the final sample depending on the metal oxide being etched. The results illustrate the importance of the co-reactant design during thermal atomic layer etching processes depending on the target material to be etched, desired processing temperature range, and the substrate.

ACKNOWLEDGMENTS

We acknowledge financial support from EMD Electronics, a business of Merck KGaA, Darmstadt, Germany. This work was performed in part at the Analytical Instrumentation Facility (AIF) at North Carolina State University, which is supported by the State of North Carolina and the National Science Foundation (Award No. ECCS-1542015). The AIF is a member of the North Carolina Research Triangle Nanotechnology Network (RTNN), a site in the National Nanotechnology Coordinated Infrastructure (NNCI).

AUTHOR DECLARATIONS

Conflict of Interest

The authors have no conflicts to disclose.

Author Contributions

Holger Saare: Conceptualization (equal); Data curation (lead); Formal analysis (equal); Investigation (lead); Methodology (equal); Writing – original draft (lead); Writing – review & editing (equal). **Wenyi Xie:** Conceptualization (equal); Formal analysis (equal); Investigation (equal); Methodology (equal); Writing – review & editing (equal). **Gregory N. Parsons:** Conceptualization (equal); Funding acquisition (lead); Project administration (lead); Supervision (lead); Writing – review & editing (equal).

DATA AVAILABILITY

The data that support the findings of this study are available from the corresponding author upon reasonable request.

REFERENCES

- ¹M. Toofan and J. Toofan, *Developments in Surface Contamination and Cleaning* (Elsevier, New York, 2015), pp. 185–212.
- ²K. Nøjiri, *Dry Etching Technology for Semiconductors* (Springer International, Tokyo, 2015).
- ³J. A. Dagata, *J. Vac. Sci. Technol. B* **5**, 1495 (1987).
- ⁴F. I. Chang, R. Yeh, G. Lin, P. B. Chu, E. G. Hoffman, E. J. Kruglick, K. S. J. Pister, and M. H. Hecht, *Proc. SPIE* **2641**, 117 (1995).
- ⁵H. F. Winters and J. W. Coburn, *Appl. Phys. Lett.* **34**, 70 (1979).
- ⁶V. Passi, U. Sodervall, B. Nilsson, G. Petersson, M. Hagberg, C. Krzeminski, E. Dubois, B. Du Bois, and J. P. Raskin, *Microelectron. Eng.* **95**, 83 (2012).
- ⁷A. Witvrouw, B. Du Bois, P. De Moor, A. Verbist, C. A. Van Hoof, H. Bender, and C. Baert, *Proc. SPIE* **4174**, 130 (2000).
- ⁸V. Lindroos, M. Tilli, A. Lehto, and T. Motooka, *Handbook of Silicon Based MEMS Materials and Technologies* (Elsevier, New York, 2010).
- ⁹P. C. Lemaire and G. N. Parsons, *Chem. Mater.* **29**, 6653 (2017).
- ¹⁰Y. Lee, C. Huffman, and S. M. George, *Chem. Mater.* **28**, 7657 (2016).
- ¹¹R. Steger and R. Masel, *Thin Solid Films* **342**, 221 (1999).
- ¹²C. T. Carver, J. J. Plombon, P. E. Romero, S. Suri, T. A. Tronic, and R. B. Turkot, *ECS J. Solid State Sci. Technol.* **4**, N5005 (2015).
- ¹³K. J. Kanarik, S. Tan, and R. A. Gottscho, *J. Phys. Chem. Lett.* **9**, 4814 (2018).
- ¹⁴K. J. Kanarik, T. Lill, E. A. Hudson, S. Sriraman, S. Tan, J. Marks, V. Vahedi, and R. A. Gottscho, *J. Vac. Sci. Technol. A* **33**, 020802 (2015).
- ¹⁵C. Fang, Y. Cao, D. Wu, and A. Li, *Prog. Nat. Sci.: Mater. Int.* **28**, 667 (2018).
- ¹⁶S. M. George, *Acc. Chem. Res.* **53**, 1151 (2020).
- ¹⁷Y. Lee and S. M. George, *ACS Nano* **9**, 2061 (2015).
- ¹⁸Y. Lee, J. W. Dumont, and S. M. George, *Chem. Mater.* **28**, 2994 (2016).
- ¹⁹A. Fischer, A. Routzahn, Y. Lee, T. Lill, and S. M. George, *J. Vac. Sci. Technol. A* **38**, 022603 (2020).
- ²⁰Y. Lee, J. W. Dumont, and S. M. George, *Chem. Mater.* **27**, 3648 (2015).
- ²¹S. Imai, T. Haga, O. Matsuzaki, T. Hattori, and M. Matsumura, *Jpn. J. Appl. Phys.* **34**, 5049 (1995).
- ²²A. I. Abdulagatov and S. M. George, *Chem. Mater.* **30**, 8465 (2018).
- ²³J. W. DuMont, A. E. Marquardt, A. M. Cano, and S. M. George, *ACS Appl. Mater. Interfaces* **9**, 10296 (2017).
- ²⁴R. Rahman, E. C. Mattson, J. P. Klesko, A. Dangerfield, S. Rivillon-Amy, D. C. Smith, D. Hausmann, and Y. J. Chabal, *ACS Appl. Mater. Interfaces* **10**, 31784 (2018).
- ²⁵J. A. Murdzek and S. M. George, *J. Vac. Sci. Technol. A* **38**, 022608 (2020).
- ²⁶Y. Lee and S. M. George, *J. Vac. Sci. Technol. A* **36**, 061504 (2018).
- ²⁷Y. Lee, J. W. DuMont, and S. M. George, *ECS J. Solid State Sci. Technol.* **4**, N5013 (2015).
- ²⁸D. R. Zywotko and S. M. George, *Chem. Mater.* **29**, 1183 (2017).
- ²⁹A. Mameli, M. A. Verheijen, A. J. M. Mackus, W. M. M. Kessels, and F. Roozeboom, *ACS Appl. Mater. Interfaces* **10**, 38588 (2018).
- ³⁰E. Mohimi, X. I. Chu, B. B. Trinh, S. Babar, G. S. Girolami, and J. R. Abelson, *ECS J. Solid State Sci. Technol.* **7**, P491 (2018).
- ³¹Y. Gong, K. Venkatraman, and R. Akolkar, *J. Electrochem. Soc.* **165**, D282 (2018).
- ³²N. Toyoda and A. Ogawa, *J. Phys. D: Appl. Phys.* **50**, 184003 (2017).
- ³³W. Xie, P. C. Lemaire, and G. N. Parsons, *ACS Appl. Mater. Interfaces* **10**, 9147 (2018).
- ³⁴N. R. Johnson and S. M. George, *ACS Appl. Mater. Interfaces* **9**, 34435 (2017).
- ³⁵Y. Lee and S. M. George, *Chem. Mater.* **29**, 8202 (2017).
- ³⁶N. Marchack, J. M. Papalia, S. Engelmann, and E. A. Joseph, *J. Vac. Sci. Technol. A* **35**, 05C314 (2017).
- ³⁷M. Konh, C. He, X. Lin, X. Guo, V. Pallem, R. L. Opila, A. V. Teplyakov, Z. Wang, and B. Yuan, *J. Vac. Sci. Technol. A* **37**, 021004 (2019).
- ³⁸J. C. Gertsch, A. M. Cano, V. M. Bright, and S. M. George, *Chem. Mater.* **31**, 3624 (2019).
- ³⁹X. Lin, M. Chen, A. Janotti, and R. Opila, *J. Vac. Sci. Technol. A* **36**, 051401 (2018).

18 July 2025 11:46:54

- ⁴⁰K. C. Chen, T. W. Chu, C. R. Wu, S. C. Lee, and S. Y. Lin, *2D Mater.* **4**, 034001 (2017).
- ⁴¹Y. Lee, N. R. Johnson, and S. M. George, *Chem. Mater.* **32**, 5937 (2020).
- ⁴²J. Li *et al.*, *Materials (Basel)* **13**, 771 (2020).
- ⁴³M. R. Aziziyani, H. Sharma, and J. J. Dubowski, *ACS Appl. Mater. Interfaces* **11**, 17968 (2019).
- ⁴⁴H. Zhu, X. Qin, L. Cheng, A. Azcatl, J. Kim, and R. M. Wallace, *ACS Appl. Mater. Interfaces* **8**, 19119 (2016).
- ⁴⁵W. Lu, Y. Lee, J. C. Gertsch, J. A. Murdzek, A. S. Cavanagh, L. Kong, J. A. Del Alamo, and S. M. George, *Nano Lett.* **19**, 5159 (2019).
- ⁴⁶N. R. Johnson, J. K. Hite, M. A. Mastro, C. R. Eddy, and S. M. George, *Appl. Phys. Lett.* **114**, 243103 (2019).
- ⁴⁷A. Ludviksson, M. Xu, and R. M. Martin, *Surf. Sci.* **277**, 282 (1992).
- ⁴⁸H. Zhou, Y.-C. Fu, M. M. A. Mirza, and X. Li, in *AVS 18th International Conference on Atomic Layer Deposition (ALD), Incheon, Korea*, 29 July–1 August 2018 (AVS, New York, 2018).
- ⁴⁹V. Sharma, T. Blomberg, S. Haukka, S. Cembella, M. E. Givens, M. Tuominen, R. Odedra, W. Graff, and M. Ritala, *Appl. Surf. Sci.* **540**, 148309 (2021).
- ⁵⁰A. Roine, T. Kotiranta, H. Eerola, and P. Lamberg, *HSC Chemistry Ver. 7.1* (Oktukumpu Research Oy, Pori, 2002).
- ⁵¹E. Lassner and W.-D. Schubert, *Tungsten: Properties, Chemistry, Technology of the Element, Alloys, and Chemical Compounds* (Springer, Boston, MA, 1999).
- ⁵²See supplementary material online for additional thermodynamic modeling data, measured film thickness values, AES spectra, and AFM images.